JOURNAL OF MATERIALS SCIENCE **36** (2001) 55–66

A microstructural study of silicon carbide fibres through the use of Raman microscopy

YANLING WARD, ROBERT J. YOUNG
Manchester Materials Science Centre, UMIST/University of Manchester, Manchester M1 7HS, UK
E-mail: robert.young@umist.ac.uk

ROBERT A. SHATWELL
Mechanical Sciences Sector, DERA, Farnborough, Hants GU14 0LX, UK

The microstructures of three different silicon carbide (SiC) fibres produced by CVD (chemical vapour deposition) have been examined in detail using Raman microscopy. Raman spectra were mapped out across the entire cross-sections of these silicon carbide fibres using an automated *x-y* stage with a spatial resolution of 1 μm. The Raman maps clearly illustrate the variations in microstructure in such types of silicon carbide fibres. It appears that the SCS-type fibres contain carbon as well as SiC whereas the Sigma 1140+ fibre also contains free silicon. Furthermore, the differences in the detailed structures of the carbon and silicon carbide present in the fibres can also be investigated. Raman microscopy is demonstrated to be a very sensitive technique for characterising the composition and microstructure of CVD silicon carbide fibres prepared using different processing conditions.

1. Introduction

There has been a growing interest in the development of silicon carbide fibres in recent years for structural reinforcement in high temperature metal- and ceramic-matrix composites. This is because silicon carbide fibres can offer high strength, high stiffness, excellent heat, oxidation and corrosion resistance and exceptional high-temperature stability. There are two major commercial methods for the production of silicon carbide fibres: one involves deposition of a silane compound on to a carbon or tungsten substrate, the other decomposition of a polymeric precursor [1]. Silicon carbide fibres produced by the chemical vapour deposition (CVD) technique usually have large diameters ranging from 100 to 150 μm and their microstructures are very sensitive to the detailed conditions of the CVD-process. It has been shown [2] that the resulting structure of the silicon carbide fibres is strongly dependent on the composition, pressure and supply rate of the vapour mixture and deposition temperature. Thus, the composition and microstructure may vary from fibre to fibre due to different deposition conditions employed during the CVD process.

In order to obtain a better understanding of these CVD fibres, it is necessary to investigate how the conditions of CVD process correlate with the microstructure of the fibres, and how the physical and mechanical properties of the fibres are related to this microstructure. A number of investigations have been carried out to identify the microstructure of CVD SiC fibres using a variety of techniques such as x-ray diffraction [3, 4], transmission electron microscopy (TEM) [5–7], Auger electron spectroscopy and parallel electron energy loss spectroscopy [4, 8], and Raman spectroscopy [4, 9]. These studies indicated that the fibres consist of different layers as a result of changes in the deposition conditions that occur during the CVD process. It is also clear that the microstructure of the silicon carbide fibres has a significant effect upon the physical and mechanical properties of fibres and final performance of such fibres within the composites [10, 11].

Raman spectroscopy has been shown to be very useful for the study of a wide range of structural characteristics of materials such as carbon and silicon. It is well understood that the position, relative intensity and bandwidth of their Raman bands are related closely to the degree of order in the structure and the stress in the material. The Raman technique also has the advantages of being very quick and efficient as well as requiring little sample preparation. The microstructure of silicon carbide fibres can be examined simply from freshly-fractured surfaces or polished sections of fibres [4, 9]. A previous study by Kim *et al*. [9] showed that Raman spectroscopy can be used successfully to identify the presence of excess carbon and silicon in silicon carbide fibres. They also demonstrated that their results were in qualitative agreement with the TEM investigations [5, 6]. In this study, we demonstrate that Raman mapping is particular useful technique to characterise the spatial variations in the composition and microstructure of three different CVD silicon carbide fibres on the micron level. Furthermore, it is shown that the results can provide valuable information about the distribution of SiC, carbon or silicon in these fibres, the

carbon structures present and the variation in crystal size or crystal perfection of silicon carbide.

2. Experimental procedure

2.1. Materials

The silicon carbide fibres examined in this study were SCS-6, SCS Ultra and Sigma SM1140+, all three produced via the chemical vapour deposition (CVD) technique. The SCS-type fibres, developed by Textron Speciality Materials Co., are made by chemical vapour deposition of silicon- and carbon-containing compounds on to a carbon core whereas the Sigma SM1140+ fibres, developed by DERA, are deposited on to a tungsten substrate.

Polished cross-sections of SCS-6 and Sigma 1140+ fibres were obtained from the fibres in a unidirectional metal matrix composite consisting of the fibres embedded in a Ti-6Al-4V alloy matrix. The SCS Ultra fibres were mounted between two pieces of glass embedded in an epoxy resin and then polished to obtain fibre cross-sections suitable for the Raman investigation.

2.2. Raman microscopy

The Raman microscopic studies were carried out on a Renishaw Raman Microscope 1000 system, using the 632.8 nm line of a 25 mW He-Ne laser as the excitation source and a highly-sensitive Peltier-cooled couple charged device (CCD) detector. The laser beam was focused to a $\sim$2 μm diameter spot on the sample using a modified Olympus BH-2 optical microscope with a $\times$50 objective lens. The laser power on the sample was kept below 2 mW to avoid any band shifts or structural modifications due to heating effects. All the Raman spectra were obtained with laser polarisation parallel to the radial direction of the fibres (unless otherwise stated) and an exposure time of about 30 s. There was no polarisation analysis of the scattered radiation. The Raman spectra were curve fitted using Lorentzian functions to determine the exact positions of the Raman bands.

3. Results and discussion

3.1. Fibre microstructures

Optical micrographs of polished cross-sections of SCS-6 and Sigma SM1140+ fibres in metal matrix composites are shown in Fig. 1. These are consistent with previous TEM studies [7, 8]. It can be seen that the SCS-6 fibres are about 140 μm in diameter and have a $\sim$30 μm diameter dark core. The fibres also have a 1–2 μm thick darker coating on outside of the core and a $\sim$3 μm thick dark outer coating on the external surface In contrast, the Sigma SM1140+ fibres have a total diameter of about 100 μm and a $\sim$15 μm diameter bright tungsten core, surrounded by darker silicon carbide deposits and a $\sim$5 μm outer coating. A change from a rough inner region to a smooth outer region can be observed at about 17 μm from edge of the core, due to a variation in microstructure of the fibre. The SCS Ultra fibres have the similar features to the SCS-6 fibres. However the higher hardness led to sample preparation difficulties, so the inner carbon coating surrounding the core and the outer carbon coating are less evident.

3.2. Raman spectra of silicon carbide (SiC) fibres

Fig. 2 displays a series of Raman spectra in the range of 300–3000 cm^{-1} obtained from different positions across the polished sections of the SCS-6, SCS Ultra and Sigma SM1140+ fibres. The spectra were obtained at intervals of 10 μm from fibre centre towards the fibre surface. Since no spectrum could be obtained from the tungsten core in the Sigma SM1140+ fibre, spectra for this fibre were obtained only from edge of the core towards surface of the fibre. It can be observed that the Raman spectra change with position for all three fibres and that the sets of Raman spectra for the three fibres are all quite different from each other. These changes in the appearance of Raman spectra are associated with variations in the microstructure of such fibres, as observed from the previous Raman studies [4, 9]. The Raman spectra shown in Fig. 2 exhibit three regions of interest:

(i) two well-defined bands at around 1330 cm^{-1} and 1600 cm^{-1} in the region 1000 cm^{-1} to 1800 cm^{-1};
(ii) a group of Raman bands between 600 cm^{-1} and 1000 cm^{-1}; and
(iii) a sharp band at 522 cm^{-1}.

The details of these Raman bands will be interpreted in detail in terms of the structure of the SiC fibres.

Two distinct Raman bands at around 1330 and 1600 cm^{-1}, are found in the core and inner region of the SCS-6 and SCS-Ultra fibres, and in the surface regions of all of the fibres. These two bands are very similar to those observed for polycrystalline graphite, amorphous carbon and a wide range of carbon fibres [12–14]. These two bands correspond to the D- and G-bands of crystalline graphite respectively [12]. The Raman band at 1600 cm^{-1} has been assigned to the E_{2g} C-C (sp^2-bonded) stretching mode of single crystal graphite. The other Raman band at 1330 cm^{-1}, not appearing in the single crystal graphite, is attributed to the A_{1g} C-C (sp^3-bonded) stretching mode and results from the crystal boundaries of polycrystalline graphite [12, 13]. Thus the presence of the 1330 and 1600 cm^{-1} bands indicates the existence of free carbon in the fibres. Furthermore it can be seen that the appearance of the 1330 and 1600 cm^{-1} bands such as the position, relative intensity, and bandwidth, is distinctly different in the fibre core compared to the inner regions of the SCS-type fibres. It can be seen that both bands change from being very sharp and intense in the fibre core to being broader and overlapping somewhat, eventually becoming weak and extremely broad band at ca. 1400 cm^{-1} (as shown by spectra (f)-(h) in SCS Ultra in Fig. 2b). A similar feature at ca.1400–1500 cm^{-1} has been observed previously in amorphous carbon films by Cho *et al*. [15]. This can be explained as a change from graphitic carbon to more disordered carbon and finally an amorphous

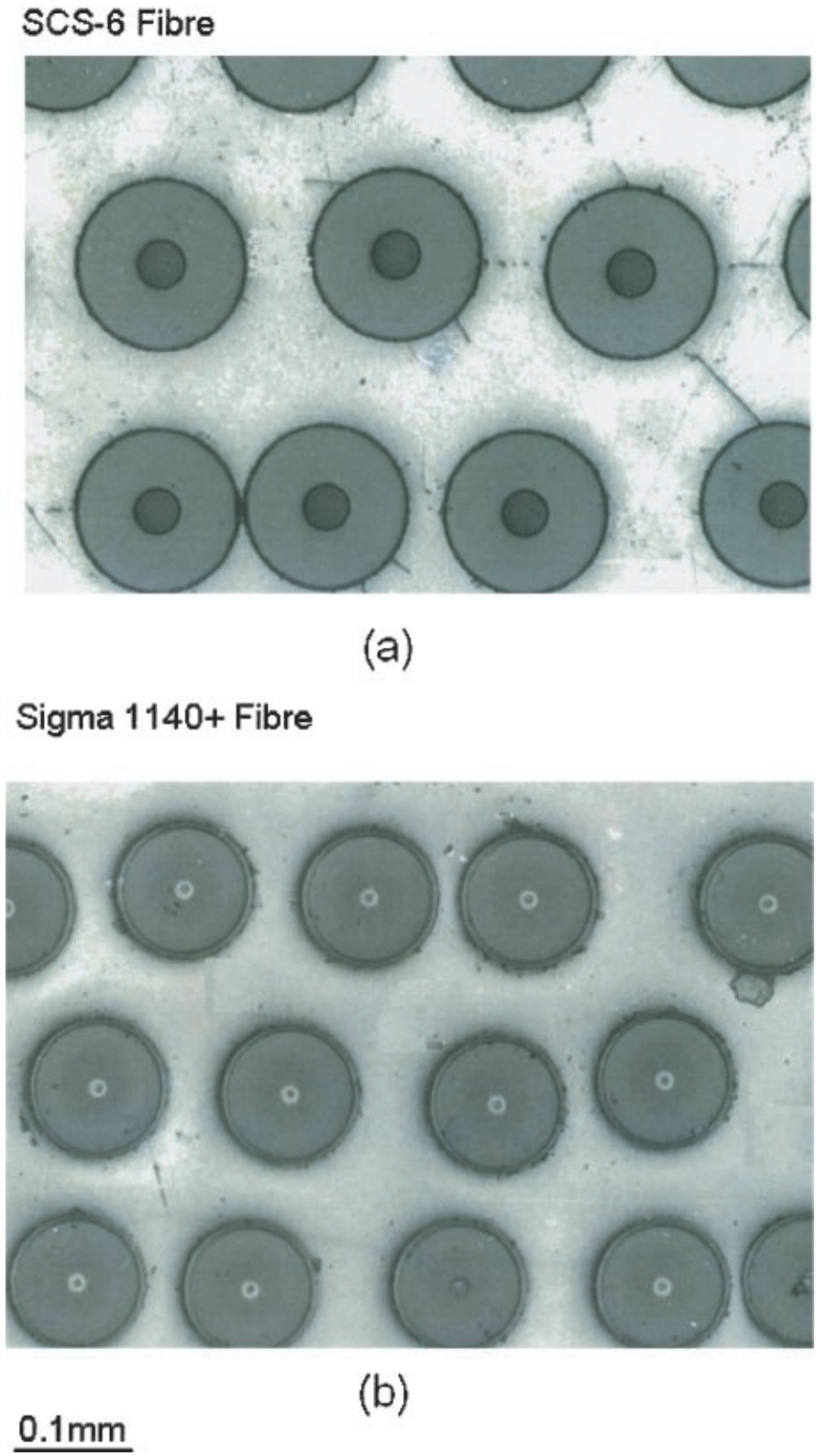

Figure 1 Optical micrographs of polished cross-sections of (a) SCS-6 and (b) Sigma SM1140+ SiC fibres in the metal matrix.

carbon structure. It is interesting to note that the spectra obtained from the core of the SCS-6 and SCS-Ultra fibres consists not only of sharp and strong 1330 and 1600 cm^{-1} bands but also additional features at about 2660 and 2900 cm^{-1}. These two bands are believed to be second-order and combination bands corresponding to 2×1330 cm^{-1} and $1330 + 1600$ cm^{-1}, which have been observed previously in the spectra of crystalline graphite, glassy carbon and high modulus carbon fibres [12–14, 16]. It has been claimed [14] that the first-order bands relate to structure order within the carbon sheets (*a*-*b* plane) whereas the second-order bands are related to the stacking disorder along the *c*-axis. The presence of second-order bands in the spectra therefore reflects the graphitic nature of the carbon structure in the fibre core.

All silicon carbide polytypes give Raman scattering from a transverse optic (TO) phonon at approximately 790 cm^{-1} and a longitudinal optic phonon (LO) at 973 cm^{-1} [17–19]. In these samples, the 973 cm^{-1}

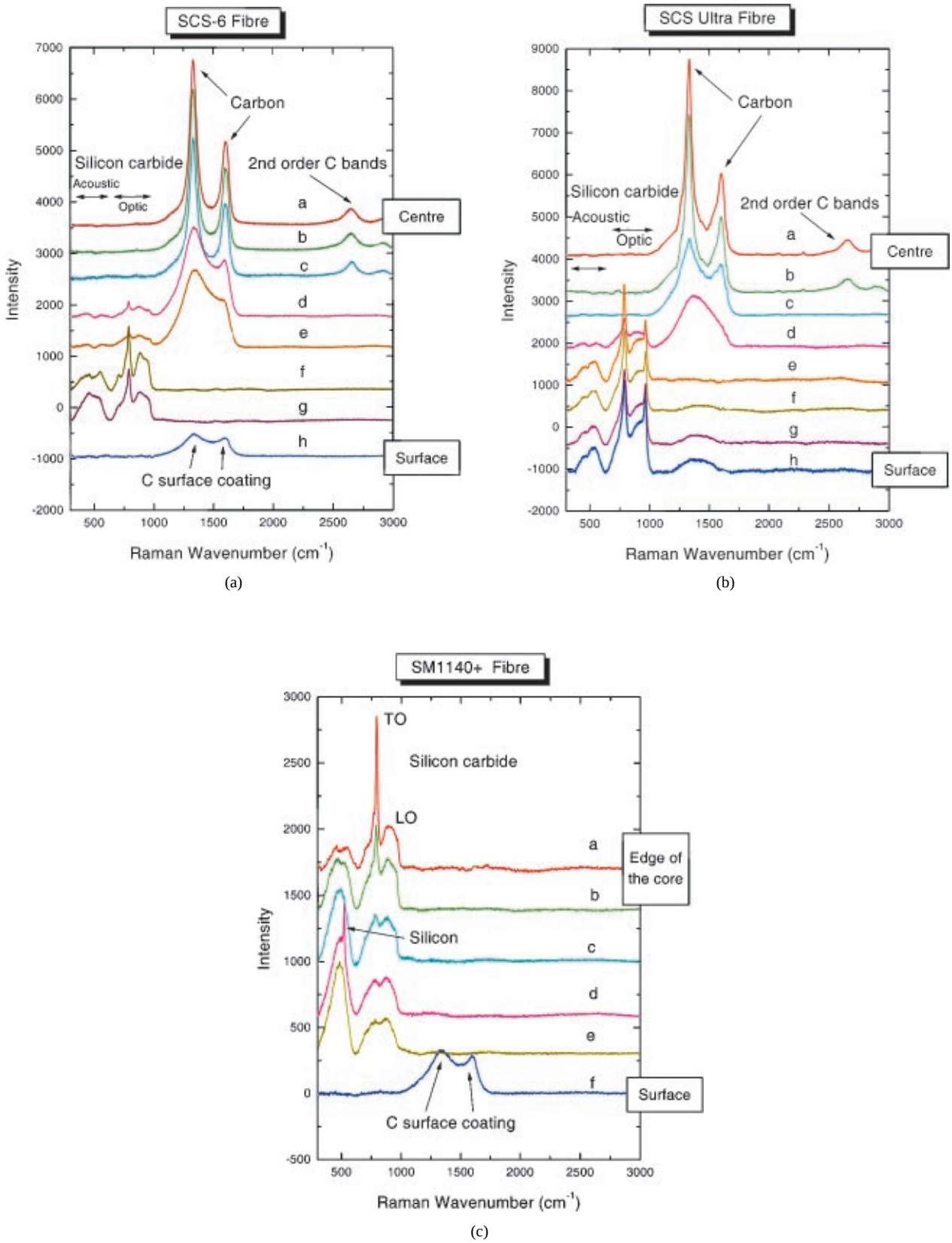

Figure 2 Raman spectra in the region 300–3000 cm^{-1} obtained at different positions across the cross-section of SiC fibres: (a) SCS-6; (b) SCS Ultra and (c) Sigma SM1140+. For comparison, all spectra have been corrected for background scattering and shifted along the intensity axis.

phonon appears shifted down to 964 cm^{-1}. This shift is independent of the wavelength of the exciting radiation and is probably due to the small crystallites found in these samples [20]. This is also consistent with the large linewidths of these transitions when compared with other work [18, 19]. Whilst the predominant SiC polytype is β- or 3C, the extensive stacking faults within the crystallites [7, 8] effectively mix other polytypes into the structure. Thus the shoulder at 765 cm^{-1} evident in all the spectra of Fig. 2 could be regarded as arising from such an admixture [21].

In addition to the above bands, all three monofilaments show Raman scattering in the 200–600 cm^{-1} region. This arises from the silicon carbide acoustic

phonons. This scattering would be forbidden in large, perfect single crystals. However, the presence of phonon scattering mechanisms leads to a breakdown of the $\Delta \mathbf{k} = 0$ selection rule and mixes phonons with different wavevectors [20, 22]. This scattering could occur at grain boundaries or at stacking faults. It has been stated that, when the average crystallite size is <10 nm, the Raman line-shape simply reflects the phonon density of states in the Brillouin zone [21]. This is the type of scattering expected from amorphous material. Thus the Raman technique is unable to distinguish between these situations.

Raman spectra from a Sigma SM1140+ fibre are markedly different from those of SCS fibres. It can be seen that spectrum (d) in Fig. 2c exhibits not only the silicon carbide bands but also a sharp band at around 522 cm^{-1}. This 522 cm^{-1} band has been ascribed to the longitudinal optical phonon (LO) mode of silicon [19]. Thus the presence of the silicon band in the spectra confirms the presence of free silicon crystals in the fibre [8]. Moreover, as well as the sharp band there is also a strong broad band with a peak just below 500 cm^{-1}. This could be due to the presence of amorphous silicon that has a TO band at 475 cm^{-1} [23].

3.3. Raman mapping

It is well known that small changes in the microstructure of fibres can affect mechanical strength of fibres and the fibre/matrix interface properties. Previous studies have shown that the presence of a small amount of carbon in SiC fibres can maintain the high strength in fibres by suppressing the growth of SiC crystals, while the presence of silicon may have an adverse effect [9, 21]. The complex microstructures observed for the SCS-6 fibre reflect the importance of the precise characterisation of these fibres, particularly at various interfaces between the core/SiC deposit, and outer coating/matrix. In this work, the point-to-point variation of Raman spectra with distance from the fibre centre to the surface can be obtained by moving the sample in intervals of 2 μm using an automated x-y stage with a spatial resolution of 1 μm. Such Raman maps can give a visual indication of exact location and form of SiC, carbon and silicon present in the fibres.

3.3.1. SCS-6 fibre

Fig. 3 shows the results of Raman mapping across an SCS-6 fibre starting from the fibre centre and moving towards the surface. All the spectra taken from the core region show only the carbon bands, indicating the fibre has a carbon core. Moving away from the fibre core to the inner region, the Raman spectra reveal the presence of SiC bands as well as the carbon bands. This confirms that this region consists of a mixture of silicon carbide and carbon. The carbon bands disappear abruptly at a distance about 45 μm away from the fibre centre and only SiC bands can be observed in this region. This is consistent with previous observations that the outer region of the fibre is made up of only stoichiometric SiC [8]. The reappearance of only carbon bands at fibre surface (70 μm from the fibre centre) confirms that the fibre has a pure carbon outer coating on its surface.

It is clear that the fibre consists of a core of 30–35 μm diameter, an inner region about 25 μm thick and an outer region about 25 μm thick, followed by a 1–3 μm coating on the fibre surface. The carbon bands in the core are intense and narrow. This indicates that the fibre core has well-ordered graphitic carbon crystallite structure. In addition to lower intensities and broader widths compared to the carbon core region, the carbon bands obtained moving away from the core show a decrease in intensity and an increase in bandwidth. On the other hand the SiC bands change very little in terms of intensity and bandwidth throughout the region. This indicates that the carbon structures in this region become more disordered. It can be seen that the Raman bands from silicon carbide in this region are often weak in the presence of carbon and sometimes, as reported previously [9], can be too weak to be detected. This can be explained by the fact that the Raman scattering efficiency of SiC is much lower than that of carbon [21].

Unfortunately the ratio of band intensities between carbon and SiC can not be used as a direct measure of the amount of carbon and SiC present in the fibre since the relative scattering efficiency of SiC compared to that of graphite is not known for the 632.8 nm line of a He-Ne laser. However the reduction in relative intensity of carbon to SiC can still be seen. This indicates that there is a subsequent decrease of amount of free carbon with increasing the distance from fibre centre, as supported by previous microanalysis on the fibre [8]. A rapid increase in intensity of the SiC bands is observed at the transition from the inner region to the outer region. The sharp and intense band at 790 cm^{-1} band assigned to SiC suggests that the silicon carbide has a much larger crystallite size compared to that in the inner region. It can also be noted that the intensity of the SiC band at 790 cm^{-1} decreases continuously with increasing the distance from the carbon core, probably associated with a decrease in the crystal size of SiC. This is supported by a previous TEM investigation that showed the crystal size of SiC is about 250 nm close to the inner region but drops to only 90 nm near the fibre surface [6]. The carbon bands from the outer coating are weak and extremely broad, indicating that carbon structure in this region is highly disordered.

3.3.2. SCS-Ultra fibre

The microstructure of the SCS Ultra fibre is clearly illustrated by the Raman mapping in Fig. 4. The spectra from the fibre core reveal only Raman bands characteristic of carbon, confirming that the fibre has a carbon core. Silicon carbide bands can be observed throughout the rest of the fibre while the carbon bands disappear at about 35 μm from the centre and re-emerge at around 15 μm from the surface. Thus the SCS Ultra fibre has three different regions, for the inner and outer regions, a mixture of carbon and silicon carbide, and for the middle region, almost stoichiometric silicon carbide.

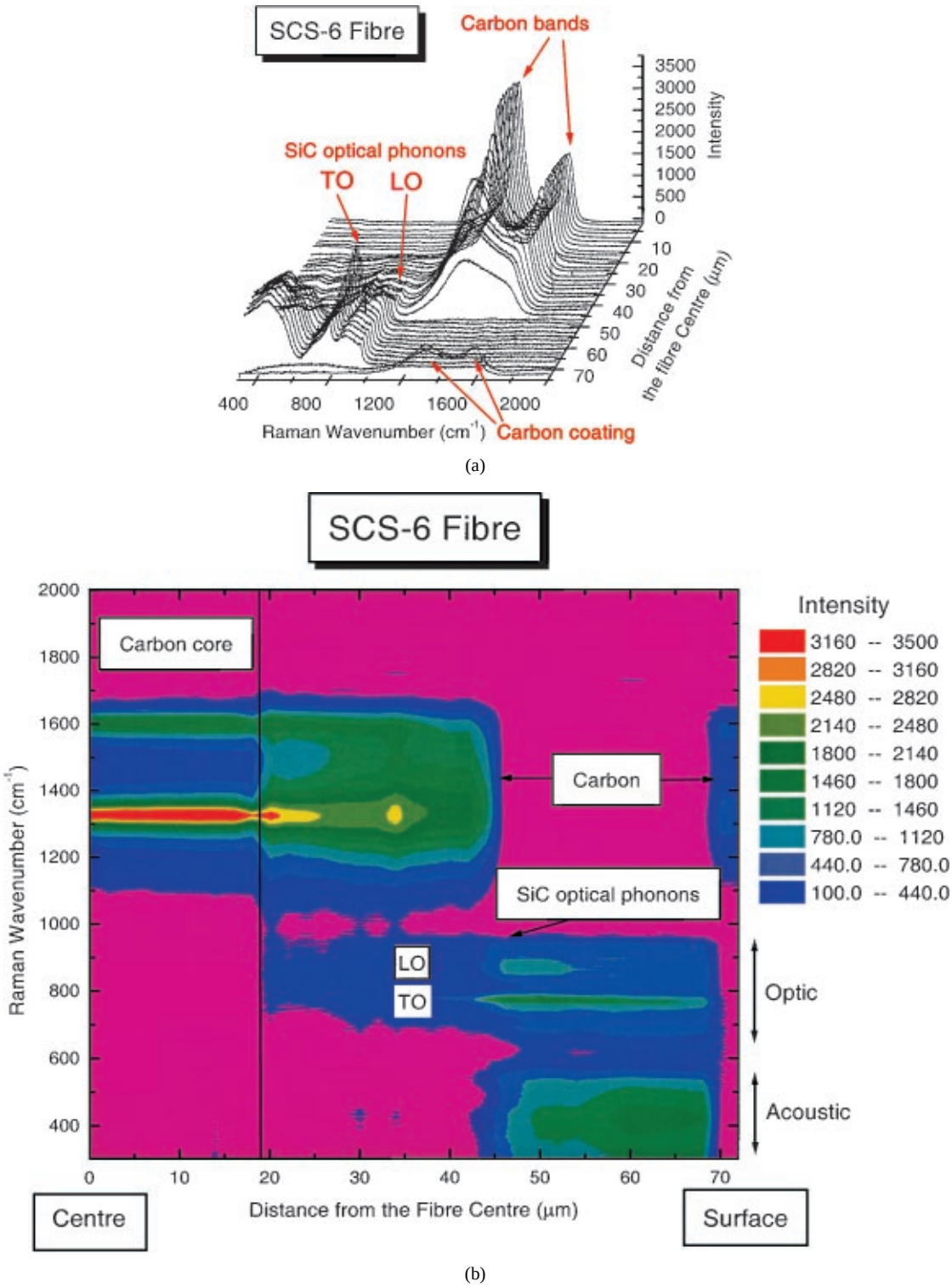

Figure 3 (a) Raman line mapping and (b) Raman scattering intensity contour map from the centre to the surface of the fibre for an SCS-6 fibre.

The carbon bands from the first 7 μm of the core are intense and, suggesting a well-defined graphitic carbon crystallite structure. Band broadening and band shift towards higher frequencies are observed as going out towards edge of the core. This means that carbon becomes more disordered near the core/SiC interface and is possibly in compression. The structures of carbon and SiC are found to be distinctly different in different regions. In the inner region, carbon near the fibre core exhibits sharp and strong bands at 1330 and 1600 cm^{-1} characteristic of well ordered graphitic carbon structure. It becomes more disordered and possibly amorphous as moving towards the fibre surface, as observed from the progressive broadening of the bands and appearance of a broad feature at 1400 cm^{-1}. On the other hand, SiC in the inner region, remains poorly crystallised with small crystal size. The middle and outer regions contain almost no carbon or only a small amount of carbon as going towards the fibre surface. SiC scattering becomes well characterised with a small degree of phonon scattering, as indicated by the relatively sharp TO and LO phonon bands at 790 and 964 cm^{-1}, when compared with SCS-6 and SM1140+.

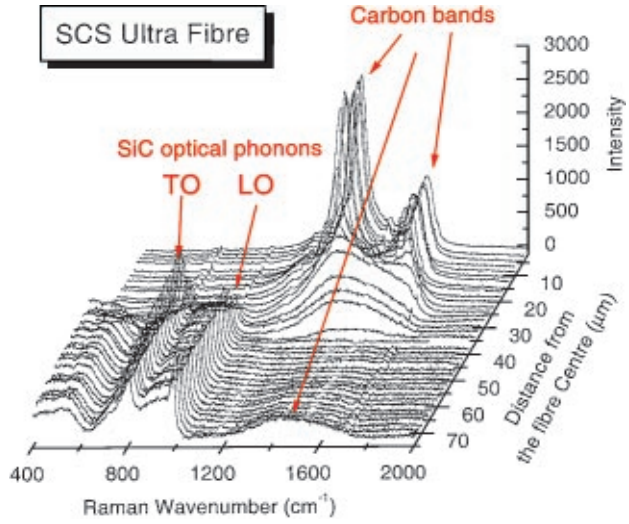

(a)

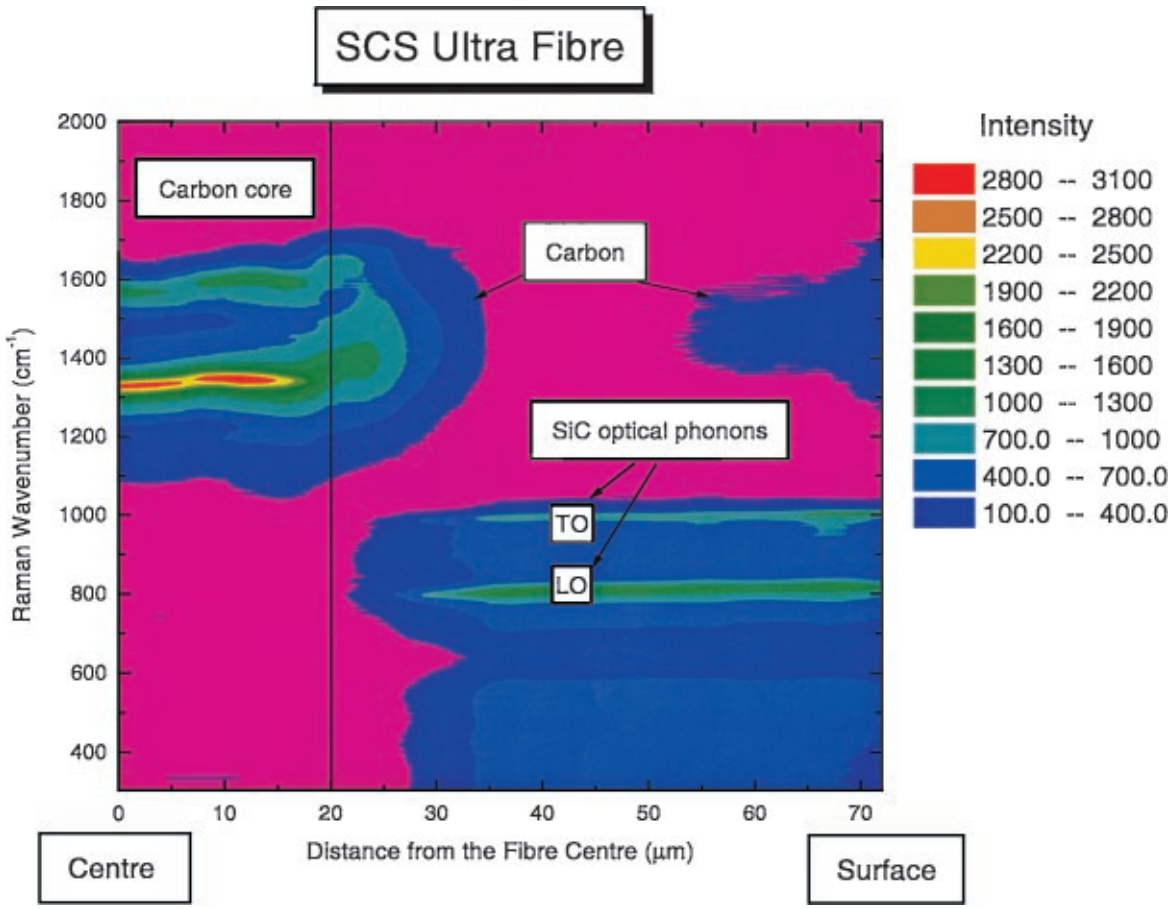

(b)

Figure 4 (a) Raman line mapping and (b) Raman scattering intensity contour map from the core to the surface of the fibre for an SCS Ultra fibre.

3.3.3. Sigma SM1140+ fibre

Fig. 5 presents the Raman mapping of a Sigma 1140+ fibre obtained from edge of the core towards the fibre surface. Raman bands assigned to carbon are absent throughout the entire fibre cross-section except at the very surface of the fibre. Only the Raman bands assigned to SiC are observed near the tungsten core, suggestive of stoichiometric silicon carbide in the region. The 522 cm^{-1} band due to silicon emerges at about 18 μm away from edge of the tungsten core, corresponding to the transition from the rough inner region to the smooth outer region in Fig. 1b. The silicon band appears almost throughout the entire outer region, except near the surface. This confirms that this region has a mixture of silicon carbide and silicon. The carbon bands are only observed on fibre surface from the outer coating, confirming that the fibre has a pure carbon coating applied on the fibre surface for the surface protection. The silicon carbide bands are very sharp and strong near the tungsten core and become broad and weak as moving out towards the fibre surface. This can be explained by the decrease in crystal size and perfection

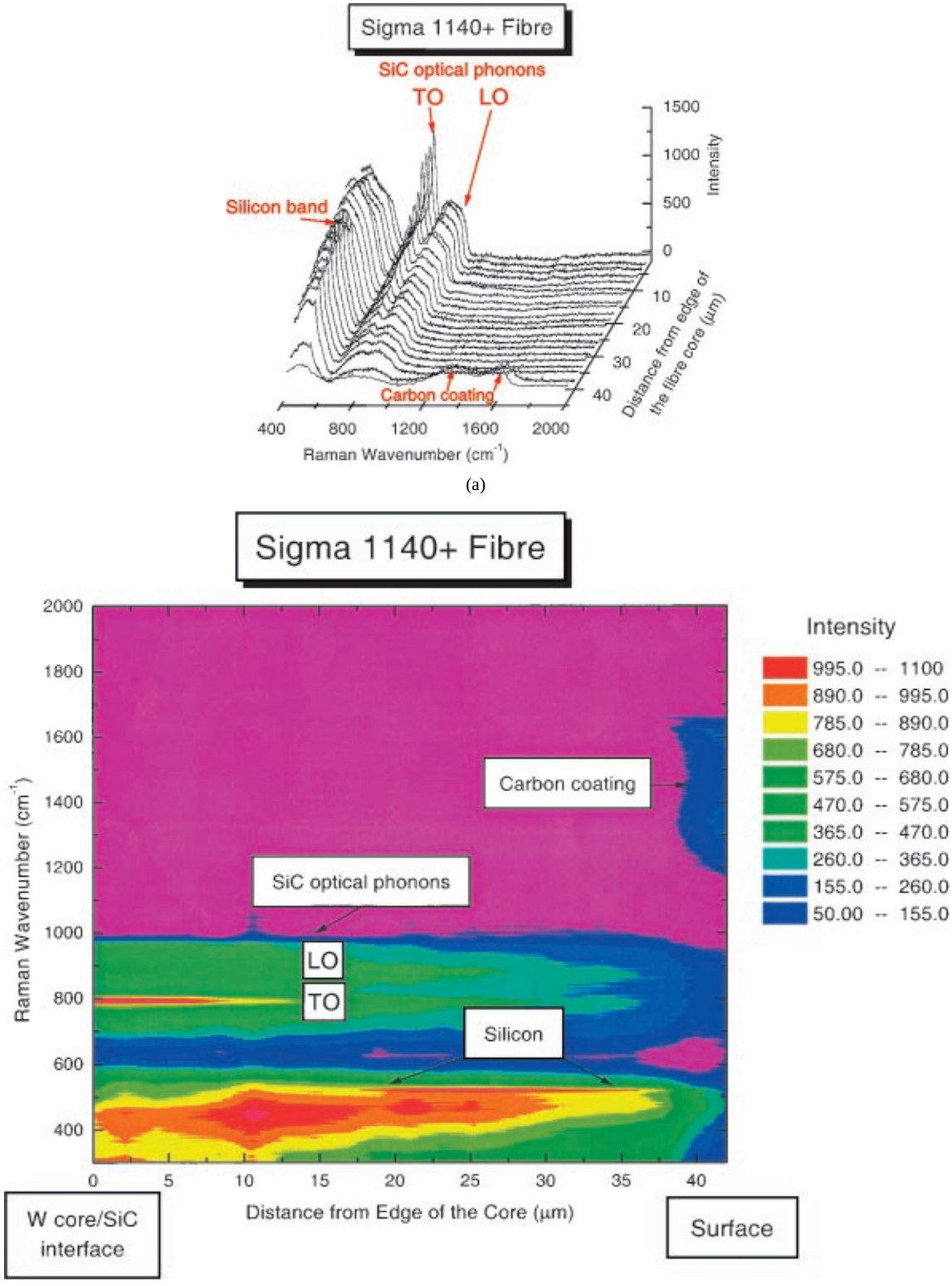

Figure 5 (a) Raman line mapping and (b) Raman scattering intensity contour map from edge of the core to the surface of the fibre for a Sigma SM1140+ fibre.

of SiC across the fibre section [7]. The appearance of the 790 cm^{-1} band near the tungsten core suggests that silicon carbide is highly crystallised with large crystal size while the band near the surface, indicates that silicon carbide is nanocrystalline or amorphous. The intensity of the silicon band increases towards the centre of the region and reaches maximum at about 25 μm from the edge of the core then drops towards the fibre surface.

3.3.4. Polarisation effects

Raman spectra were also obtained from the SCS-6 fibre with the polarisation of laser beam perpendicular to the radial direction of the fibre. It is known that the existence of anisotropic structures could result in anisotropic mechanical properties in fibres. The Raman mapping on the same SCS-6 fibre with the laser polarisation perpendicular to the radial direction of the fibre is shown in Fig. 6. A difference between Figs 3 and 6

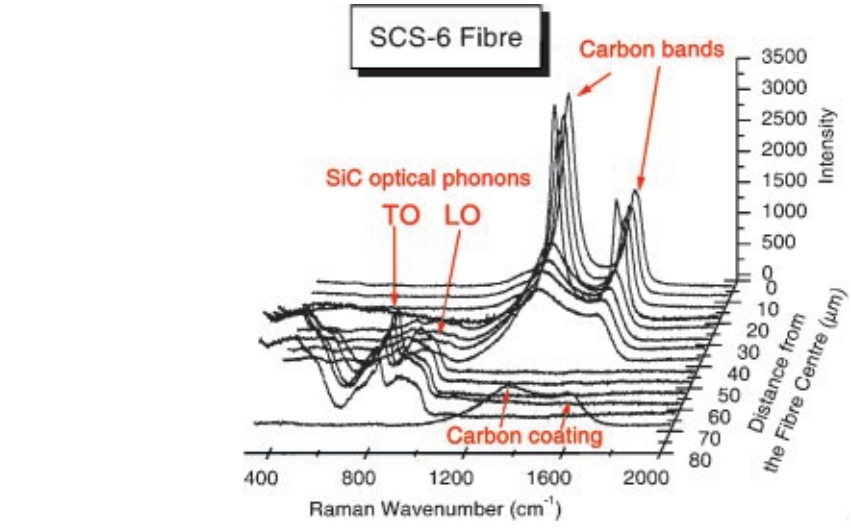

(a)

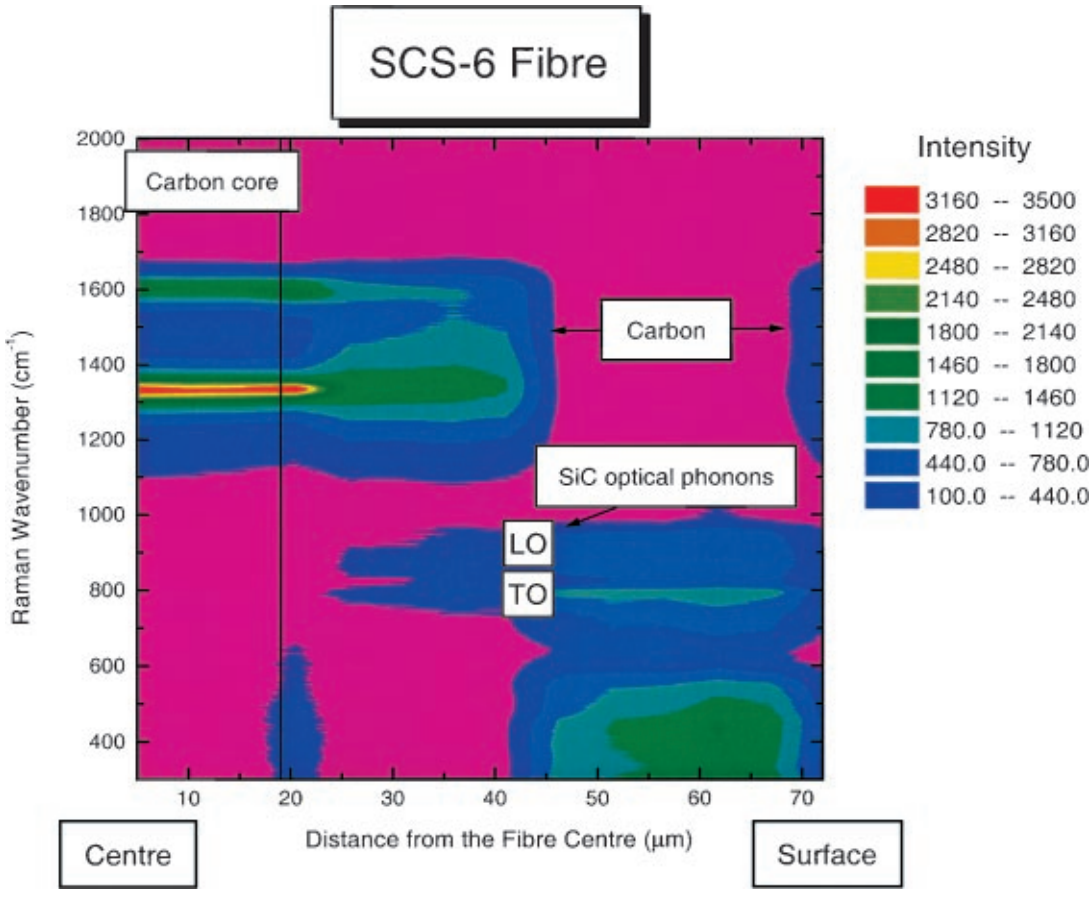

(b)

Figure 6 (a) Raman line mapping and (b) Raman scattering intensity contour map from the core to the surface of the fibre for an SCS-6 fibre. In this case the laser beam was polarised perpendicular to the radial direction of the fibre.

can be observed and they clearly reflect the anisotropic structures present in the fibre. The carbon bands from the inner coating are different from those of the carbon core. They are also narrower and stronger than those seen from the inner coating in Fig. 3. This can be explained by that the graphite planes in the inner carbon coating being oriented preferentially perpendicular to the radial direction of the fibre rather than randomly rotated as in the carbon core and carbon in the inner region. It can also be observed from Fig. 3 that the SiC band at 790 cm^{-1} is very strong and narrow near the inner region and becomes weak and broad towards the surface. Whereas the 790 cm^{-1} band in Fig. 6 is almost the same throughout the outer region with the intensity and bandwidth similar to those observed near the fibre surface in Fig. 3. This implies that the SiC crystallites in the fibre are not oriented randomly, but have a degree of alignment parallel to the radial direction of the fibre.

Our Raman analysis is in qualitative agreement with the TEM observation on the same fibre by Ning *et al.* [6].

3.4. Comparison of Raman scattering from the different fibre types

Raman spectra of these fibres exhibit distinct features associated with crystalline and amorphous SiC, carbon with different structure forms and silicon, revealing that such fibres contain not only silicon carbide but also free carbon and silicon. The spectra reveal that the SCS-type fibres have a graphitic carbon core and consist of a mixture of silicon carbide and carbon whereas the Sigma SM1140+ fibre contains a mixture of silicon carbide and silicon. Our results also demonstrate that Raman spectroscopy can be used to distinguish carbon structures and states of crystallisation of silicon carbide in the fibres which has been found to be very difficult with other methods [3, 6]. The technique can be performed simply on polished cross-sections of fibres using scan times of the order of minutes.

3.4.1. SiC line-shapes

One-phonon Raman scattering from a perfect crystal should only detect the optical phonons at the centre ($\mathbf{k} = 0$) region of the Brillouin zone [24]. In silicon carbide this would give two sharp, strong bands at 796 and 972 cm^{-1}. In hexagonal or orthorhombic polytypes, additional weaker bands would be observed in their vicinity [17, 19]. The classification of phonon states by wavevector applies only if they are truly de-localised over the entire lattice. If any mechanism exists that confines the phonons to a restricted volume, or scatters them, the wavevector classification breaks down and with it the $\Delta\mathbf{k} = 0$ selection rule for one-phonon transitions [20–22].

The extreme case of the above happens in the amorphous state. The wavevector, **k**, no longer has any meaning and all phonons are optically allowed. In this case, the Raman spectrum is broad and shifted to low frequency. The shape of the Raman band reflects the density of phonon states in the Brillouin zone [20–22]. An additional consequence of this breakdown of long-range order is the appearance of scattering from acoustic phonons from the outer regions of the Brillouin zone. (Acoustic phonons have zero frequency at the zone centre.)

In their study of polycarbosilane-based SiC fibres heat treated at different temperatures, Sasaki *et al.* [21] observed similar spectra to those shown here. Fibre heat treated at the highest temperature (1500 °C) looked similar to the SiC in the inner regions of SM1140+. Fibres heat treated at lower temperatures showed very weak, broad bands in the acoustic and optical phonon regions. Sasaki indicated that, when the crystallite size was less than 10 nm, the spectrum would be indistinguishable from the amorphous state.

It is evident that the SiC scattering from all monofilaments studied here shows significant relaxation of the $\Delta\mathbf{k} = 0$ selection rule associated with one-phonon Raman transitions and that scattering from the outer regions of SM1140+ and SCS-6 could be regarded as arising from either the amorphous state or crystallite smaller than 10 nm, using the Sasaki criterion. Similarly, the relatively sharp optic phonon SiC scattering from SCS-Ultra and comparatively weak acoustic phonon scattering indicate lower phonon scattering and by implication, larger crystallite size.

This interpretation is, however, too simplistic. Whilst, in SM1140+, the crystallite size does decrease with increasing radius, it is generally greater than 10 nm [7]. Similarly SCS-6 has crystals between 90–1000 nm long throughout its structure [6, 8]. Conversely, SCS-Ultra, that shows the best-defined phonon spectrum, has smaller crystallites than any other monofilament [25, 26]. However, TEM does show that stacking faults are present in the silicon carbide in all these monofilaments and the stacking fault separation can be of the order of tens of nanometres. It therefore appears that the Raman scattering is looking at phonon confinement *within* a crystal, in addition to that at the crystal boundaries. This could be due to stacking faults or other imperfections not readily observable by TEM [27].

This study indicates therefore that the SiC phonon scattering is less for SCS-Ultra than the other monofilaments studied and implies that the stacking fault density is correspondingly reduced. The spectra suggest that this could be related to the co-deposition of carbon, since the carbon-rich inner region of SCS-6 in Fig. 3b shows a lower acoustic phonon scattering than the outer region or than any regions of SM1140+ (Fig. 5b). By implication, the SiC in this region shows less phonon confinement. However, the SCS-Ultra scattering is significantly different from that of SCS-6, so co-deposition of carbon in itself does not bring about the modification in microstructure.

It could be argued that co-deposition of silicon has the opposite effect on defects within the SiC. The appearance of the silicon peak in SM1140+ is concurrent with an increase in intensity of the acoustic phonon band and a more amorphous appearance of the optical bands. This effect could equally be due to the reduced crystallite size coincident with the co-deposition of silicon.

It was decided to determine if the SiC Raman line-shape in SCS-Ultra could be analysed quantitatively. Models have been developed to analyse the intermediate state between scattering from perfect single crystals in which only $\mathbf{k} = 0$ phonons are observed, and scattering from the amorphous state where all phonons are seen.

Richter, Wang and Ley [20] were the first to consider the effects on the Raman spectrum if crystallite size was gradually reduced, effectively localising the phonons in space. They applied their model to the LO Raman band in silicon. Tiong *et al.* [27] showed that the model could also explain localisation induced by damage to the crystal. They explained the modification of the line-shape of an LO phonon in GaAs induced by progressive amounts of ion implantation damage. The model has been used extensively to explain the Raman line-shapes found in nano-crystalline semiconductor materials. Petrovic *et al.* [28] explained qualitatively the Raman spectra of different SiC whiskers using the same ideas.

Two effects are observed as phonon confinement by whatever mechanism increases:

- The Raman lineshape becomes asymmetric, acquiring a low frequency "tail".
- The energy of the transition decreases.

The model developed by Richter *et al*. [20], normally referred to as the RWL model, assumes that the phonon transition is still basically centred around $\mathbf{k} = 0$ in the Brillouin zone, but the phonon eigenfunctions in this region have been modified to include a small admixture of $\mathbf{k} \neq 0$ phonons. A damping function weights the mixing of these other phonons into the $\mathbf{k} = 0$ eigenstate. The model basically applies a small perturbation to the normal de-localised phonon model. The net result is the following expression for the Raman intensity at angular frequency ω:

$$I(\omega) = \int_0^1 \frac{d^3k|C(0,k)|^2}{(\omega - \omega(k))^2 + (\Gamma_0/2)^2} \qquad (1)$$

where:

- $|C(0,k)|^2$ is a weighting coefficient controlling the admixture of the eigenfunctions of wavevector $\mathbf{k}$ into those with wavevector 0.
- $\omega(k)$ is the function describing the dispersion of the phonon in the Brillouin zone [17, 19].
- Γ_0 is the linewidth of the undistorted Raman line.
- The integration is over the Brillouin zone.

Various weighting function have been tried. The one that agrees best with the results on silicon and gallium arsenide [27] is Gaussian in form:

$$|C(0,k)|^2 = \exp\left\{\frac{-k^2L^2}{16\pi^2}\right\} \qquad (2)$$

The use of the extended Brillouin zone means that k is a dimensionless parameter ranging from 0 to 1 [17]. Similarly L is a dimensionless parameter where $L = 1$ [1] corresponds to the distance between the nearest-neighbour Si (or C) planes. However, it is best to regard it as an empirical parameter, particularly since there is little theoretical justification for the form of the weighting function.

In this work, a model was constructed to simultaneously fit the TO and LO phonon bands of SiC. Phonon dispersion data from Feldman *et al*. [17, 19] for TO and LO phonons were plotted and cubic polynomials fitted to the results. They fitted the spectra of all SiC polytypes to a common phonon dispersion curve in an extended Brillouin zone. This is the approach adopted here.

The model produces a line-shape that, at high values of L gives two distinct phonon peaks. At low L values, the TO phonon peak shows little change but the LO phonon peak is broadened asymmetrically to low wavenumber. Significant changes are seen for L varying between 10 and 100. As a rough guide this can be interpreted as representing a range of 10 to 100 interplanar spacings, but the error bars on these numbers could be large.

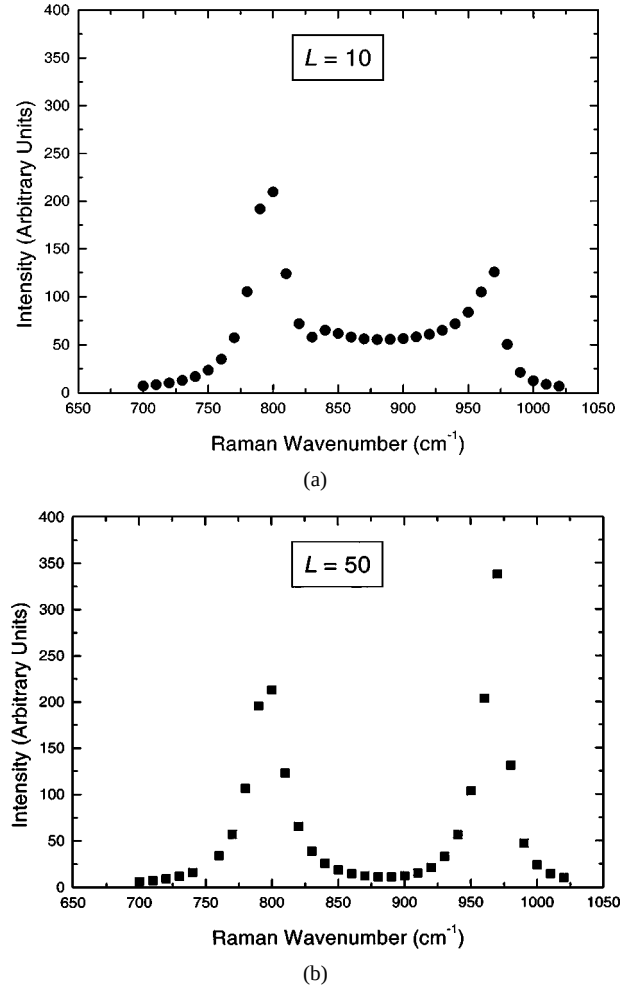

Figure 7 Predicted SiC Raman line-shape for (a) $L = 10$ and (b) $L = 50$.

Fig. 7a shows the predicted lineshape for $L = 10$. Comparison with Fig. 2b shows it to be a reasonable likeness of the polarised Raman spectrum of the SiC in SCS-Ultra. The experimental spectrum shows a low frequency shoulder on the TO phonon band that the model does not predict. The model, however, assumes inherently that the perfect crystal would be a 3C, polytype. If a hexagonal or orthorhombic polytype should be the starting point for the model, some extra bands would exist. When L is increased to 50, the model predicts a spectrum having two distinct, relatively sharp bands consistent with a 3C structure (Fig. 7b).

Variation of the correlation length, L, affects the LO phonon far more the TO phonon. This is because the dispersion of the LO phonon is four times greater than that of the TO phonon. The LO scattering intensity can therefore be spread out over a much larger range of frequencies by varying L. There is very little modification to the line-shape for values of $L < 10$ in this simulation. The model assumes a small deviation for perfect translational symmetry and so cannot reproduce the line-shapes found for SM1140+ and SCS-6.

4. Conclusions

Raman microscopy has proven to be a valuable non-destructive technique for characterising the microstructures of SiC fibres. Raman bands characteristic of SiC,

carbon and silicon have been observed in silicon carbide fibres at different positions across the fibre diameter, revealing that the microstructure of SiC fibres is not uniform because of changing deposition conditions during growth of SiC fibre. It appears that the SCS-6 fibre is made of an inner region of a mixture of silicon carbide and an outer region of stoichiometric SiC. The SCS Ultra fibre has a more complex structure with three different regions, a mixture of silicon carbide and carbon near the carbon core, surrounded by almost pure stoichiometric SiC then followed by an outer region of silicon carbide and a very small amount of amorphous carbon. The Sigma 1140+ fibre appears to be made of an inner region of pure stoichiometric SiC and an outer region of a mixture of near amorphous silicon carbide and silicon. The information gained on the distribution of SiC, carbon or silicon in these fibres, and the structure of SiC, particularly at various interfaces (core/SiC, SiC/outer coating and outer coating/matrix) can be very important for optimising fibre strength and fibre-matrix interface properties in the composites. It is interesting to note that the well-defined SiC bands can also be used to monitor fibre internal stresses inherited from CVD process and residual stresses in the composites; this will be reported in future publications.

Acknowledgements

The authors are grateful to the EPSRC for financial support and to Prof. P. Bowen of University of Birmingham for providing samples of the SCS-6 composite.

References

1. C. H. ANDERSSON and R. WARREN, *Composites* **15** (1984) 16.
2. F. CHRISTIN, R. NASLAIN and C. BERNARD, Proc. The 7th Inter. Conf. on CVD. edited by T. O. Sedwick and H. Lydtin (1979) p. 499.
3. R. T. BHATT and D. R. HULL, *Ceram. Eng. Sci. Proc.* **12** (1991) 1832.
4. P. MARTINEAU, M. LAHAYE, R. PAILLER, R. NASLAIN, M. COUZI and F. CRUEGE, *J. Mater. Sci.* **19** (1984) 2731.
5. X. J. NING, P. PIROUZ, R. D. LAGERLOF and J. DICARLO, *J. Mater. Res.* **5** (1990) 2865.
6. X. J. NING and P. PIROUZ, *ibid.* **6** (1991) 2234.
7. T. T. CHENG, I. P. JONES, R. A. SHATWELL and P. DOORBAR, *Mat. Sci. & Eng.* **A260** (1999) 139.
8. X. J. NING, P. PIROUZ and S. C. FARMER, *J. Amer. Ceram. Soc.* **76** (1993) 2033.
9. J. KIM, S. TLALI, H. E. JACKSON, J. E. WEBB and R. N. SINGH, *J. Appl. Phys.* **82** (1997) 407.
10. M. K. BRUN and M. P. BOROM, *J. Amer. Ceram. Soc.* **72** (1989) 1993.
11. E. LARA-CURZIO, S. S. STERNSTEIN, C. R. HUBBARD, B. CAVIN and W. PORTER, *Mater. Sci. Engg.* **A172** (1993) 167.
12. F. TUINSTRA and J. L. KOENIG, *J. Chem. Phys.* **53** (1970) 1126.
13. D. S. KNIGHT and W. B. WHITE, *J. Mater. Res.* **4** (1989) 385.
14. P. LESPADE, R. AL-JISHI and M. S. DRESSELHAUS, *Carbon* **20** (1982) 427.
15. N. H. CHO, K. M. KRISHNAN, D. K. VEIRS, M. D. RUBIN, C. B. HOPPER, B. BHUSHAN and D. B. BOGY, *J. Mater. Res.* **5** (1990) 2543.
16. R. J. YOUNG, *J. Text. Inst.* **86** (1995) 360.
17. D. W. FELDMAN, J. H. PARKER JR., W. J. CHOYKE and L. PATRICK, *Phys. Rev.* **173** (1968) 787.
18. H. OKUMURA, E. SAKUMA, J. H. LEE, H. MUKAIDA, S. YOSHIDA and K. ENDO, *J. Appl. Phys.* **61** (1987) 1134.
19. J. H. PARKER, D. W. FELDMAN and M. ASHKIN, *Phys. Rev.* **155** (1967) 712.
20. H. RICHTER, Z. P. WANG and L. LEY, *Solid State Comm.* **39** (1981) 625.
21. Y. SASAKI, Y. NISHINA, M. SATO and K. OKAMURA, *J. Mater. Sci.* **22** (1987) 443.
22. M. H. BRODSKY and M. CARDONA, *J Non-Crystalline Solids* **31** (1978) 81.
23. T. TANAKA, E. MARUYAMA, T. SHIMADA and H. OKAMOTO, "Amorphous Silicon" (John Wiley & Sons Ltd., Chichester, 1999) p. 78.
24. R. LOUDON, *Advan. Phys.* **13** (1964) 423.
25. A. CHATTERJEE, J. R. ROESSLER, L. E. BROWN, P. W. HEITMAN and G. E. RICHARDSON, "Microstructure and Mechanical Properties of Ultra SCS Fiber Reinforced Orthorhombic Ti-22Al-26Nb Composites" Structural Intermetallics 1997. edited by M. V. Nathal, R. Darolia, C. T. Liu, P. L. Martin, D. B. Miracle, R. Wagner and M. Yamaguchi (TMS1997).
26. J. C. GOLDSBY, H. M. YUN and J. A. DICARLO, *Scripta Materialia* **37** (1997) 299.
27. K. K. TIONG, P. M. AMIRTHARAJ, F. H. POLLAK and D. E. ASPNES, *Appl. Phys. Lett.* **44** (1984) 122.
28. J. F. DiGREGORIO, T. E. FURTAK and J. J. PETROVIC, *J. Appl. Phys.* **71** (1992) 3524.

Received 13 December 1999
and accepted 4 April 2000